processes

MDPI

Article

Simulation and Optimization of Highly Efficient Sound-Absorbing and -Insulating Materials

Xiao Liu [1], Chengyuan Wu [2,*], Haopeng Wang [1], Wangqiang Xiao [3] and Zhiqin Cai [3]

[1] CHN Energy Zhunneng Group Co., Ltd., Ordos 010300, China; xiao.liu.aa@ceic.com (X.L.); 20035006@chnenergy.com (H.W.)
[2] School of Chemical Engineering and Technology, China University of Mining and Technology, Xuzhou 221008, China
[3] School of Aerospace Engineering, Xiamen University, Xiamen 361005, China; wqxiao@xmu.edu.cn (W.X.); caizhiqin@xmu.edu.cn (Z.C.)
* Correspondence: ts23040096a31@cumt.edu.cn

Abstract

Although crucial transport equipment in coal mining enterprises, tubular belt conveyors cause serious noise pollution. In this paper, the sound absorption and isolation performance of three kinds of highly efficient sound-absorbing and -insulating materials were studied by finite element multiphysics field software COMSOL and acoustic tests, and the structure of highly efficient sound-absorbing and -insulating materials was optimized and designed. The results show that the acoustic superstructure plate has an excellent sound insulation effect of 36 dB, and achieves an excellent sound absorption coefficient of 0.95 at 210 Hz on the acoustic simulation test. The simulated weighted sound insulation of acoustic metamaterial plate is 37 dB, and the simulated weighted sound insulation of acoustic metamaterial plate filled with particle material is 42 dB, which improves the sound insulation effect by 4~7 dB after filling with particle material, and the comprehensive absorption coefficient of the high-frequency noise of more than 800 Hz reaches 0.94, and it can effectively absorb and block the low-frequency noise as well; rock wool acoustic panels in the 500 Hz to achieve a better acoustic capacity, the absorption coefficient of 0.8 or more, but the low-frequency noise acoustic capacity is still lacking, and can not be a good solution to the full-frequency band of the acoustic problem. It can be seen that the acoustic metamaterial plate has the best sound absorption and insulation effect. At the same time, the acoustic metamaterials based on the honeycomb structure are optimized, and the sound absorption and insulation structure with the angle of 60° of the inclined plate and the length of 693 mm of the inclined plate is the optimal structure. It provides a solution to the noise pollution caused by tubular belt conveyors.

Keywords: highly efficient sound-absorbing and -insulating materials; acoustical superstructure; acoustic metamaterials; particle damping

check for updates

Academic Editor: Andrea Petrella

Received: 12 February 2025
Revised: 13 March 2025
Accepted: 18 March 2025
Published: 16 September 2025

Citation: Liu, X.; Wu, C.; Wang, H.; Xiao, W.; Cai, Z. Simulation and Optimization of Highly Efficient Sound-Absorbing and -Insulating Materials. *Processes* **2025**, *13*, 2947. https://doi.org/10.3390/pr13092947

Copyright: © 2025 by the authors. Licensee MDPI, Basel, Switzerland. This article is an open access article distributed under the terms and conditions of the Creative Commons Attribution (CC BY) license (https://creativecommons.org/licenses/by/4.0/).

1. Introduction

Noise pollution can cause harm to people, animals, instruments and meters, etc. Noise hazards mainly include: damage to hearing, inducing a variety of diseases, and impact on work and life [1]. For coal enterprises, equipment operation noise is unavoidable, equipment power, operation noise, mainly medium and high frequency, spreading distance, wide impact on the surrounding life and work of the residents will produce persistent interference, it is easy to induce a variety of diseases. As a crucial transport equipment

in coal mining enterprises, the tubular belt conveyor is prone to vibrations and noise due to various factors such as the difficulty in achieving a smooth installation of the supporting devices, friction between the conveyor belt and the rollers, and issues related to the materials and rigidity of the drive system of the conveyor [2]. At present, coal enterprises mainly reduce noise by adding silencers in the propagation process, installing soundproofing devices such as soundproofing panels and fully enclosed acoustic enclosures. The method has limited vibration damping effect and is obviously difficult to meet the requirements [3].

Highly efficient sound-absorbing and -insulating materials can effectively solve the noise pollution problem. Researchers have conducted extensive studies on acoustic metamaterials [4–8]. Zhang et al. [9] proposed a porous plate-based metamaterial that avoids the impact of pre-stretching of membranes on the acoustic performance of the metamaterial while maintaining excellent low-frequency sound insulation properties. Dogra et al. [10] proposed a design of acoustic metamaterials panels with built-in Helmholtz resonators, which can effectively reduce the weight of the material panels and at the same time provide better noise reduction. Jang et al. [11] proposed a film-based sound insulation material and found that due to the vibrations within the membrane, the structural acoustic radiation of the insulation material could be easily adjusted, making broadband sound insulation possible. Different types of scatterers used to improve acoustic absorption have been investigated by Lance et al. [12] The results show more pronounced differences in attenuation between the different types of scatterers and provide an outlook on future research priorities. Xiao et al. [13] introduced a multi-band stop laminated acoustical superstructure, designed by connecting a periodic array of mass–spring–damper subsystems, which exhibited outstanding sound insulation performance.

COMSOL finite element multiphysics software is highly effective for acoustic simulation research [14–19]. Lu et al. [20] used COMSOL software to simulate and experimentally validate membrane-based acoustic metamaterials, optimizing the distribution of eccentric masses to improve acoustic performance. Tang et al. [21] built an acoustic propagation model for tubular structures based on acoustic metamaterials using COMSOL and found that, after low-loss wavefront propagation, most of the incident sound waves were absorbed by the model and reconverged with the transmitted sound waves on the opposite side of the model. Han et al. [22] used the COMSOL finite element method to simulate the propagation characteristics of sound waves within structures, showing that plane sound waves incident on M-shaped, L-shaped, and S-shaped curved waveguide models would propagate directionally after being controlled at the resonant frequency.

This study conducts simulation research and experimental verification on three types of highly efficient sound-absorbing and -insulating materials: acoustical superstructure panels, acoustic metamaterial panels, and rock wool sound insulation panels. By comparing these materials, the optimal sound-absorbing and -insulating material is identified. Additionally, simulations of different sound insulation screen structures based on the honeycomb-structured acoustic metamaterial panel are conducted, and the results are compared with field measurements of sound insulation screens to identify the most effective sound-absorbing and -insulating structure for optimizing the design of highly efficient sound-absorbing and -insulating materials.

2. Methods

2.1. COMSOL Simulation

The simulation of acoustical superstructure panels, acoustical metamaterial panels, and rock wool sound-absorbing and -insulating panels was conducted using the acoustics

module of COMSOL (comsol multiphysics v.6.2, COMSOL Co., Ltd., Shanghai, China) and the acoustics-structure coupled frequency-domain analysis module.

2.1.1. Acoustical Superstructure Panel Model and Parameters

A finite-area type superstructure was designed based on the fundamental frequency of the conveyor belt system. The material used was aluminum alloy, with the total thickness of the soundproof panel being 12 mm. The panel consisted of two outer plates and a cylindrical scattering body embedded within. The dimensions of the panel were 500 mm by 500 mm, with the outer diameter of the cylinders being 34 mm and the inner diameter 30 mm. The cylinders were arranged in a 13 × 13 periodic pattern. The acoustic superstructure panel is shown in Figure 1.

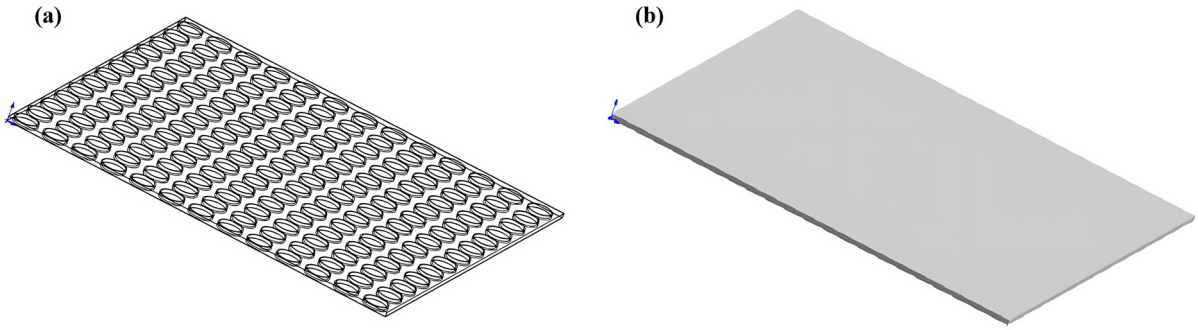


Figure 1. The superstructure sound insulation plate. (**a**) Perspective view of the acoustic superstructure panel. (**b**) Solid drawing of the acoustic superstructure plate.

2.1.2. Acoustic Metamaterial Panel Model and Parameters

In this study, the soundproofing performance of the sample was simulated using COMSOL finite element software, utilizing the acoustics-structure coupled frequency-domain analysis module for modeling and computation. The finite element simulation model is shown in Figure 2. The material parameters of the unit cells are listed in Table 1.

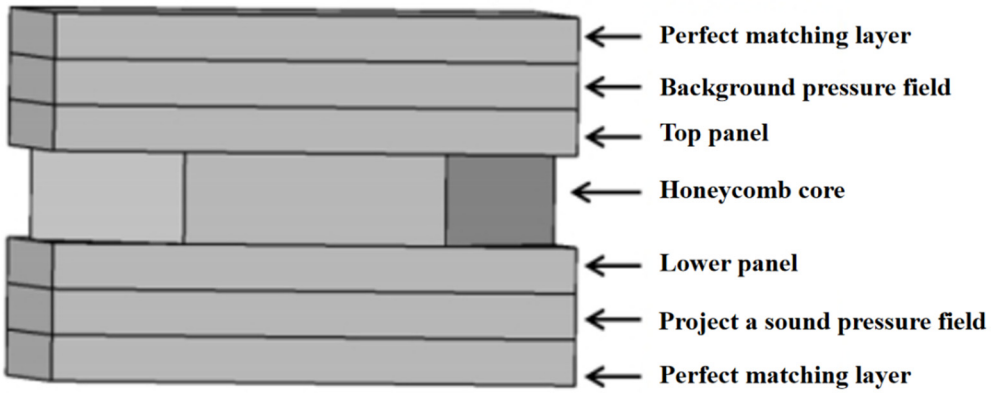


Figure 2. Cell simulation model.

Table 1. Material parameters of the unit.

Material	Density (g/cm^3)	Modulus of Elasticity (Pa)	Poisson's Ratio
Aluminum	2.7	7×10^{10}	0.33

2.1.3. Rock Wool Sound-Absorbing and -Insulating Panel Model and Parameters

The rock wool sound-absorbing and -insulating panel consists of two layers of iron-based materials and one layer of rock wool. The middle layer is made of rock wool. The

dimensions of the iron plates are 1 m × 1 m × 1 mm, while the rock wool dimensions are 1 m × 1 m × 100 mm. The model of the rock wool sound-absorbing and -insulating panel is shown in Figure 3.

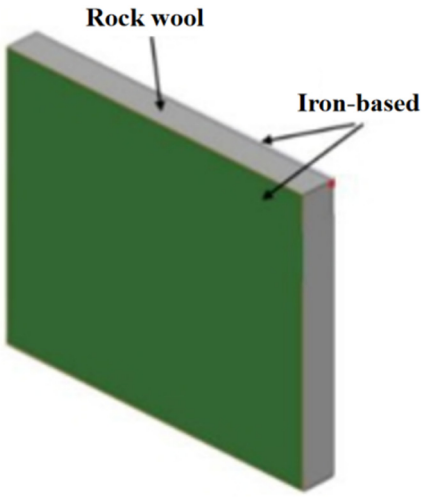


Figure 3. Model of the rock wool acoustic insulation plate.

2.2. Acoustic Test Methods

The acoustic testing setup for sound insulation and absorption is designed as shown in Figure 4. A 1000 × 1000 mm window is created in the partition wall between two rooms, A and B, for placing soundproof samples. A spherical sound source is arranged 1 m away from the partition in Room A. The input noise excitation for the spherical sound source is derived from noise data collected from a conveyor belt, simulating the noise generated by the conveyor belt on-site. A sound pressure sensor is placed 1 m away from the partition in Room B. After installing the soundproof panels, a simulation test is conducted externally in Room B to measure the sound insulation and absorption data. Tests are carried out using acoustical superstructure panels, acoustic metamaterial panels, and rock wool soundproof panels.



Figure 4. Acoustic insulation test experimental device.

Figure 5 shows the physical drawings of the three acoustic panels. The physical object of the acoustic superstructure panel used is shown in Figure 5a, which has a dimension of 1 m × 1 m × 12 mm, and its internal single cell is a diffuser with an outer diameter of 60 mm and an inner diameter of 56 mm, and its material is aluminum profile. The acoustic metamaterials panels used are physically shown in Figure 5b, with dimensions

of 1 m × 1 m × 35 mm, with a honeycomb core of a positive hexagonal shape with a side length of 4 mm, a wall thickness of 1 mm, upper and lower panels with a thickness of 1 mm, and an overall material of aluminum filled with metal damping particles. The rock wool sound-absorbing panels used are shown in Figure 5c in kind, with a size of 1 m × 1 m × 100 mm, and the material consists of two layers of 1 mm iron-based material with 100 mm rock wool.

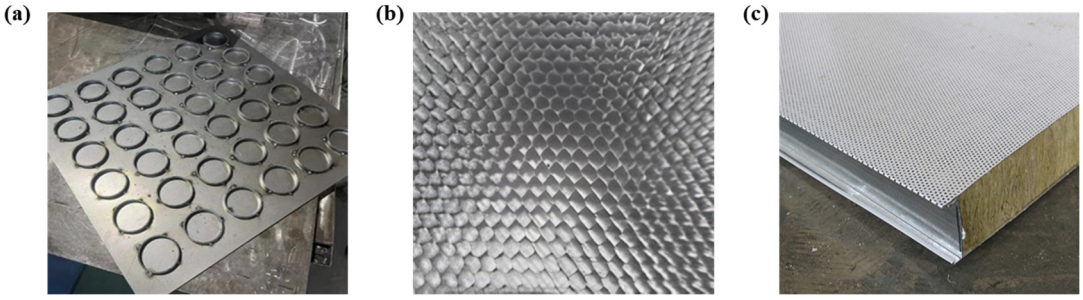


Figure 5. Acoustic panel construction. (**a**) The acoustic superstructure plate. (**b**) The acoustic metamaterial panel. (**c**) The rock wool acoustic panel.

This acoustic test was measured using an INV9212 sound pressure transducer (Coinv, Beijing, China), and the main instrumentation is shown in Table 2.

Table 2. Measuring device.

Instrument Model	Instrument Name	Instrument Description
DASP-V11	Engineering Edition Platform Software	Signal Oscilloscope Sampling, Basic Signal Analysis
INV3062W	32-bit Microvibration Collector	High acquisition accuracy and stable baseline
INV9212	Sound Pressure Sensor	High-Performance Electret Capacitive Test Sensors

2.3. VA ONE Simulation

The VA ONE software's (ESI VA ONE v.2023.5) finite element-boundary element hybrid method is employed for the acoustic optimization of highly efficient sound-absorbing and -insulating metamaterial panels. A 3D model of the tubular belt conveyor is established based on the conveyor's on-site structure, followed by a reasonable mesh division to generate a finite element model, as shown in Figure 6.

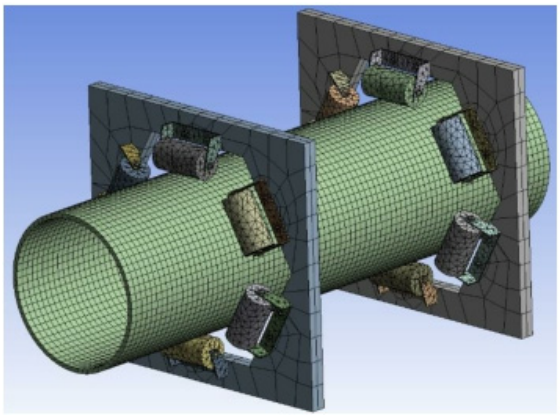


Figure 6. Finite element model of a tubular belt conveyor.

The excitation source required for the simulation is measured using an online contact force measurement system on the idler rollers. These data, combined with engineering mechanics theory, are used to calculate the time-domain signal of the idler roller force. After processing through filtering and fast Fourier transform (FFT), the force spectrum data for the idler rollers are obtained.

Since the sound pressure level at the monitoring points is jointly influenced by the tubular belt conveyor, the sound pressure level sensors are arranged according to the structural characteristics of the tubular belt conveyor. Based on the distribution pattern of the idler groups and the conveyor frame, the sound pressure levels detected by the sensors are superimposed using a sound pressure level addition method. This results in the total sound pressure level at the monitoring point within the influence range of the tubular belt conveyor. The simulation model for the soundproof screen of the tubular belt conveyor is shown in Figure 7.

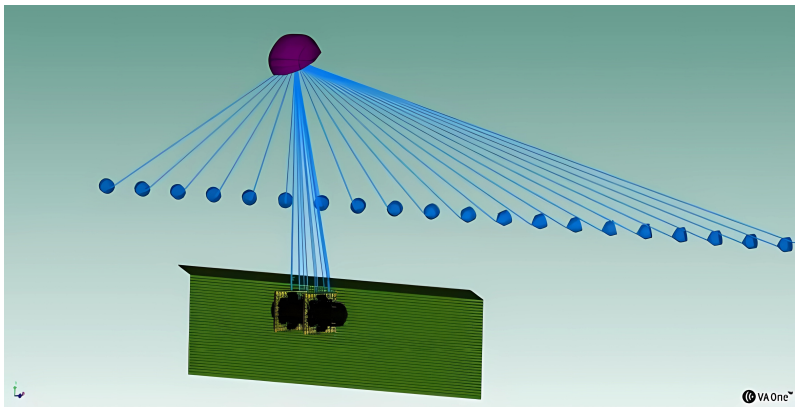


Figure 7. Finite element and boundary element hybrid sound field model of sound insulation screen of a tubular belt conveyor.

3. Results and Discussion

3.1. Acoustic Superstructure Panel Sound Insulation and Absorption Simulation Analysis

3.1.1. Acoustic Superstructure Bandgap Simulation Analysis

The superstructure is a new type of artificial periodic structure, which can be divided into Bragg scattering superstructure and local resonance superstructure according to its bandgap formation mechanism. The Bragg scattering mechanism states that the periodic structure between the cells plays a dominant role, and focuses on the analysis of the elastic or acoustic wave propagation mechanism in the structure, numerical simulation, and experimental work, and the formation of the bandgap is mainly dependent on the characteristics of the substrate material, differences in physical properties of the scatterer and the substrate, array form, filling rate, etc., and the bandgap frequency corresponds to a wavelength comparable to the transverse wave wavelength scale. The formation of band gap mainly depends on the properties of the substrate material, the difference in physical properties between the scatterer and the substrate, the array form, the filling rate, etc., and the band gap frequency corresponds to a wavelength comparable to the transverse wave wavelength scale. The localized resonance (LRSM) theory was first proposed in 2000, in which lead spheres are encapsulated in a soft silicone rubber material and arranged in an epoxy resin matrix to form a simple periodic three-dimensional cubic structure of the superstructure (LRSM). Due to the hard core wrapped in the extra-soft rubber, a resonant bandgap can be generated in the ultra-low-frequency range, and the purpose of controlling the low-frequency wave propagation by the small structure size can be realized, which is beyond the limitation of the size of the superstructure of the Bragg scattering

mechanism type [23]. Compared with the Bragg scattering mechanism, the local resonance mechanism considers that the bandgap is generated by the coupling between the resonance modes of the scatterer and the vibration modes of the substrate, and the local resonance coupling between a single scatterer and the substrate is the key factor for the generation of the bandgap.

The modeling and simulation of the band gap of the superstructure were carried out using COMSOL, resulting in the band gap diagram of the acoustical superstructure. The causes of the band gap and the conditions for the formation of a complete band gap were analyzed, validating the rationality and scientific accuracy of the superstructure modal resonance band gap theory.

As shown in Figure 8, when the excitation frequency increases from 1 Hz to the first-order natural frequency of 103 Hz, the lattice remains in the primary mode, with no attenuation and no band gap formation. As the excitation frequency approaches the second-order natural frequency of 203 Hz, vibrations continue to propagate according to the mode without generating a band gap. Similarly, when the excitation frequency approaches the third-order natural frequency of 210 Hz, vibrations continue propagating in the mode without band gap formation. However, when the excitation frequency reaches the fourth-order natural frequency of 284 Hz, the scatterers are excited into the primary mode, and the Z-direction of the scatterers couples with the plane of the substrate, thereby suppressing the elastic waves in the substrate, resulting in the formation of a complete band gap.

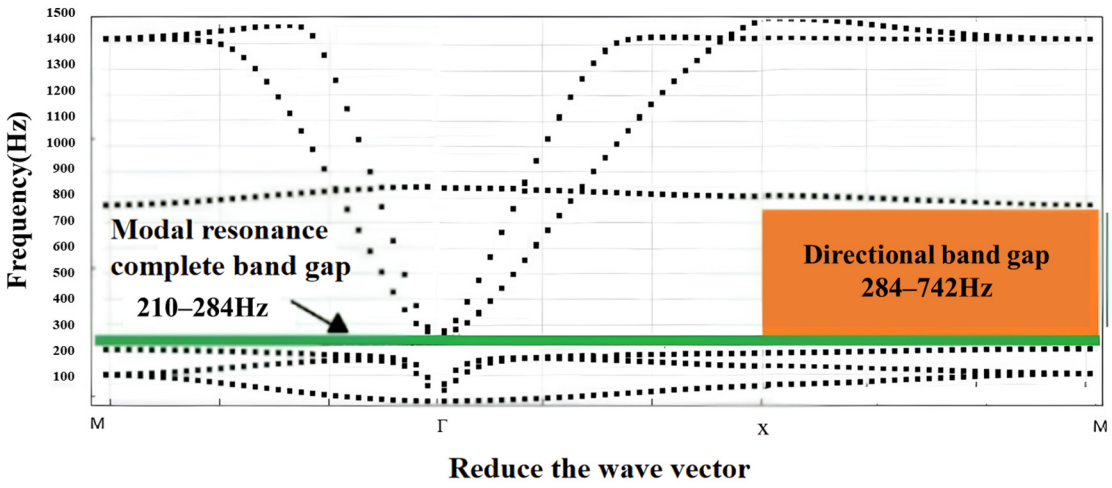


Figure 8. Acoustic superstructural bandgap.

When the excitation approaches the fourth-order natural frequency, the substrate experiences a certain degree of suppression, creating a band gap from the X to M direction. No band gap is formed when the excitation frequency exceeds the fourth-order mode. This indicates that when the excitation frequency approaches a specific natural frequency, the vibration modes of the substrate and the scatterer exhibit different responses. When the scatterer is excited to its dominant mode, the propagation of elastic waves is blocked. As shown in Figure 7, the band gap of the acoustical superstructure plate is located near the main frequency of the pipe band machine. According to the theory of acoustical superstructure band gaps, waves cannot propagate within the band gap region, which effectively reduces noise.

3.1.2. Acoustical Superstructure Sound Insulation Simulation Analysis

The acoustical superstructure panel was simulated using COMSOL software. Since the primary frequency of the tubular belt conveyor ranges from 270 Hz to 450 Hz, the noise source used in the simulation corresponds to the source noise of the conveyor. Figure 9 shows the simulation model of the superstructure unit cell.

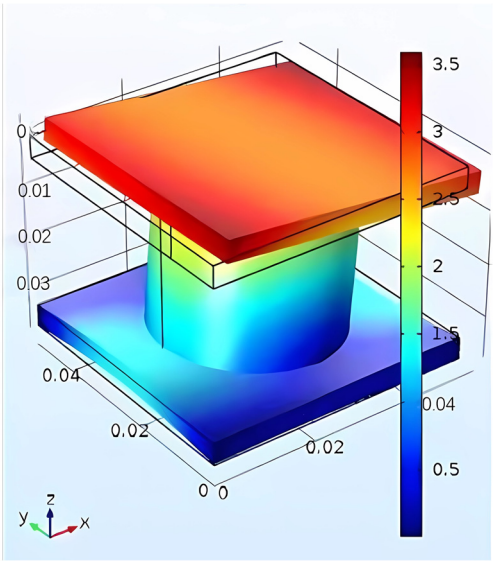


Figure 9. Hyperstructure cell simulation model.

Figure 10 presents the sound insulation curve for the acoustical superstructure panel. As shown in Figure 10, within the frequency range of 250 Hz–500 Hz, the sound waves fall within the complete band gap and directional band gap of the superstructure, which excites the scatterers. The scatterers, when excited, enter the primary vibration mode, and their *Z*-axis vibrations are coupled with the planar vibrations of the matrix. This coupling suppresses the elastic wave vibrations of the matrix, forming a complete band gap, and preventing waves from propagating through the sound insulation panel. This significantly reduces the noise transmission path, resulting in an effective sound insulation performance, with a weighted sound reduction index of 32 dB.

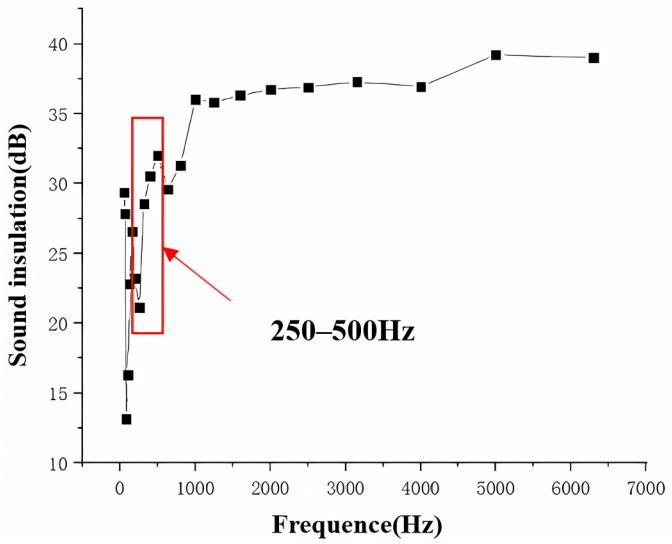


Figure 10. The sound insulation curve of the acoustic superstructure plate.

3.1.3. Acoustical Superstructure Sound Absorption Simulation Analysis

Figure 11 illustrates the sound absorption curve of the acoustical superstructure panel. As observed, due to the band gap of the acoustical superstructure panel ranging from 210 Hz to 750 Hz, it exhibits excellent sound absorption properties within this frequency range. When the sound source frequency falls between 210 Hz and 700 Hz (low-frequency noise), the region band gaps of the acoustical superstructure panel effectively enhance the sound absorption coefficient, bringing it to over 0.9. According to the theoretical and simulation results of the superstructure modal resonance band gap, the overall sound absorption performance of the acoustical superstructure panel exceeds 0.9, with excellent absorption capabilities in the low-frequency range as well, demonstrating its efficient sound absorption for mid-to-high-frequency noise. Additionally, the presence of band gaps in the acoustical superstructure panel helps suppress matrix vibration elastic waves, forming a complete band gap where waves cannot propagate through the sound insulation panel. This leads to a rapid increase in the sound absorption coefficient, maintaining excellent sound absorption even at higher frequencies.

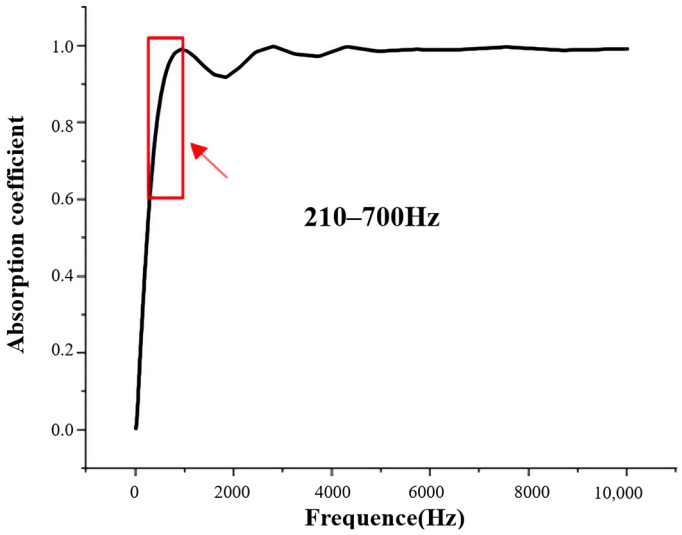


Figure 11. The acoustic absorption curve of the acoustic superstructure plate.

3.2. Acoustical Metamaterial Panel Sound Absorption and Insulation Simulation Analysis

3.2.1. Influence of Core Cell Edge Length on Sound Insulation Performance of the Metamaterial Panel

The effect of different core cell edge lengths in the acoustical metamaterial panel with a honeycomb core structure on its sound absorption and insulation performance is investigated. Figure 12 shows the three-dimensional models of the acoustical metamaterial panels, where the core height is 25 mm, and the core cell edge lengths (L) are 3 mm, 4 mm, and 5 mm, respectively. The models for the three different edge lengths were imported into COMSOL for simulation. Figure 13 presents the simulation results.

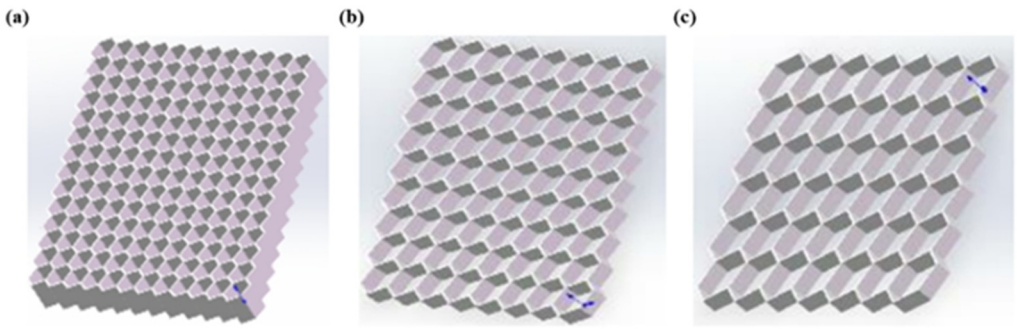


Figure 12. 3D modeling of acoustic metamaterial panels with honeycomb cores of different edge lengths. (**a**) L = 3 mm. (**b**) L = 4 mm. (**c**) L = 5 mm.

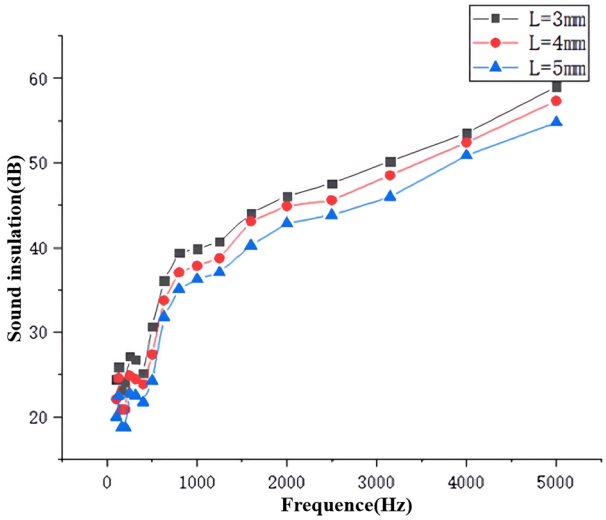


Figure 13. Sound insulation curves of acoustic metamaterial panels with honeycomb cores of different side lengths.

The sound insulation curves of acoustic metamaterial panels with honeycomb cores of different side lengths are shown in Figure 13. From the graph, it can be observed that within the specified frequency range, as the frequency increases, the sound insulation curves gradually rise with changes in the core cell edge length. At low frequencies, the curves exhibit more significant fluctuations. The frequency locations of the sound insulation peaks and valleys for different core cell edge lengths are largely the same, and the panels show good sound insulation performance within the frequency range of the tubular conveyor. As the edge length of the core increases, the sound insulation performance decreases. This is mainly because, as the core cell size increases, the number of core cells per unit area decreases, which reduces the bonding strength and shear stiffness between the core layer and the top and bottom panels. During use, this may lead to a higher risk of core adhesive failure. When subjected to large loads, the structure may fail due to insufficient strength, which further deteriorates the sound insulation performance. Additionally, this may lead to sound penetration through the top and bottom panels, further reducing the insulation. However, when the core cell edge length is small, the number of unit cells in the acoustical metamaterial panel increases, leading to more complex manufacturing processes and higher costs, placing greater demands on equipment. Therefore, considering the performance and manufacturing requirements, the panel design adopts a core cell edge length of 4 mm. Simulation results indicate that within the frequency range of the tubular conveyor, the sound insulation performance reaches its peak at 315 Hz, with a sound insulation value of

up to 24.5 dB. The overall weighted sound insulation index is 34 dB, providing a direction for determining the optimal structural parameters for the acoustical metamaterial panel.

3.2.2. Influence of Honeycomb Core Height on the Sound Insulation of Material Panels

To explore the impact of honeycomb core height on the sound insulation performance of acoustical metamaterial panels, while keeping the side length of the honeycomb core and the thickness of the top and bottom plates constant, only the height of the honeycomb core is varied. The side length of the honeycomb core is uniformly set to L = 4 mm, and three honeycomb core heights of 20 mm, 35 mm, and 50 mm are modeled, as shown in Figure 14. The acoustical metamaterial panel models for these three dimensions are imported into COMSOL for simulation, and the simulation results are shown in Figure 15.

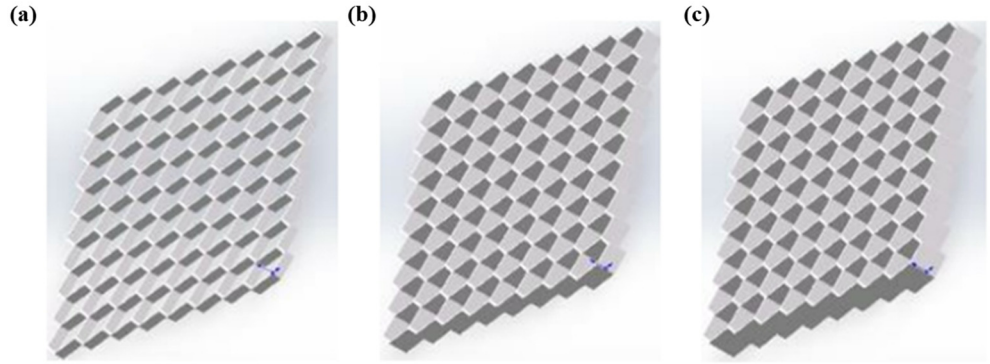


Figure 14. 3D modeling of acoustic metamaterial panels with honeycomb cores of different heights. (**a**) H = 25 mm. (**b**) H = 30 mm. (**c**) H = 35 mm.

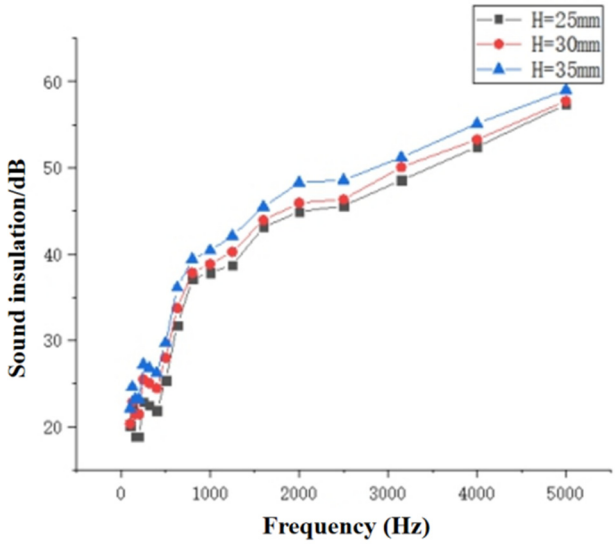


Figure 15. Sound insulation curves of acoustic metamaterial panels with honeycomb cores of different heights.

From the figure, it can be observed that for honeycomb cores of different heights, the sound insulation curves of the acoustical metamaterial panels show generally consistent trends. In the low-frequency range, the curves fluctuate more significantly, with the sound insulation increasing as the height of the honeycomb core increases. The sound insulation in the frequency range of the ducted fan is also higher. According to the sound insulation characteristics curve, when the height of the honeycomb core increases, both the stiffness and mass of the acoustical metamaterial panel as a whole are enhanced. When

the thickness of the acoustical metamaterial panel increases, more sound wave energy is reflected and dissipated within the honeycomb core, thereby improving the overall sound insulation performance. However, with increasing height, the rate of increase in sound insulation decreases, and the weight and cost of the panel also rise. To optimize sound insulation performance and improve sound insulation efficiency, considering factors such as design and cost, a honeycomb core height of 35 mm is chosen. As shown in the figure, within the frequency range of the ducted fan, the sound insulation is greatest at a height of 35 mm, with the highest sound insulation occurring at a frequency of 315 Hz, reaching 27.2 dB. The overall weighted sound insulation is 37 dB. Therefore, by adjusting the side length and height of the honeycomb core, the sound-absorbing and -insulating performance of the acoustical metamaterial panel can be effectively improved to meet practical design requirements.

3.2.3. The Effect of Particle Damping on the Sound Insulation of Material Panels

The particle damping technique is introduced into the acoustical metamaterial panel with a honeycomb core structure. By filling the cavities within the acoustical metamaterial with particulate materials to form dampers, and utilizing the associated particle motion within the material to dissipate energy, the sound-absorbing and -insulating performance is significantly enhanced. The relevant parameters of the damping particles are listed in Table 3.

Table 3. Damper particle parameters.

Material	Filling Rate (%)	Diameter (mm)
Iron base alloy	90	1.5

A discrete element–finite element coupled calculation method is employed, treating the particle system as numerous discrete units, while the sound insulation unit is analyzed using the finite element method to calculate its response. The internal stress and deformation of each mesh element are solved using the linear finite element method. The contact forces between the damping particles and the outer wall of the honeycomb core cavity, modeled as triangular shell elements, are shown in Figure 16. It can be observed that on each triangular shell element, there are collisions involving one or more particles. To effectively couple this with the finite element method, the damping force must be converted to node loads: the transformation from the shell element's local coordinates to those of the acoustical metamaterial panel model, as well as the conversion of surface element loads to node forces on triangular elements, is carried out using shape function methods. After the conversion, the forces at the nodes are applied as new boundaries in the dynamic calculation of the acoustical metamaterial panel. This allows the particle damper's effect on the sound-absorbing and -insulating unit to be represented. The simulation model of the unit filled with particles is shown in Figure 17.

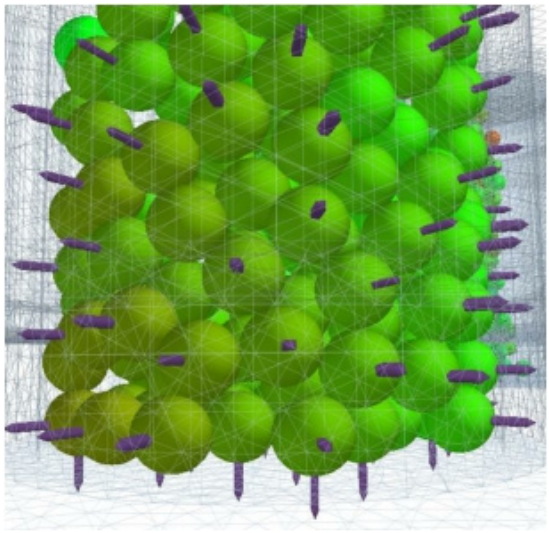


Figure 16. Contact force of triangular shell element.

The sound pressure level results of the acoustic metamaterial unit with particles added at a frequency of 315 Hz, as simulated in COMSOL, are shown in Figure 18. From the figure, it is evident that the noise from the ducted fan is effectively reduced after being treated with the particle-filled acoustic metamaterial unit.

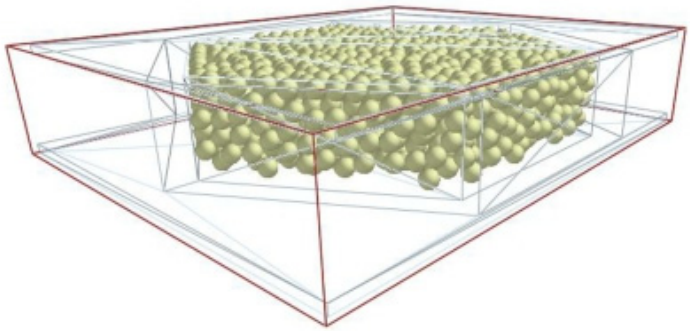


Figure 17. Simulation modeling of acoustic metamaterial unit body filled with particles.

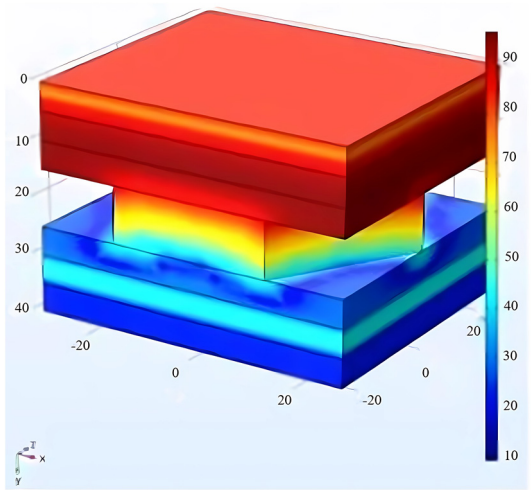


Figure 18. Simulated sound pressure level cloud of the acoustic metamaterial plate unit body.

Using a discrete element method (DEM)—finite element method (FEM) coupling approach, the particle system is treated as many discrete units, with the response of each

unit calculated using the COMSOL FEM method. The simulated sound insulation curve of the unit after filling with particles is shown in Figure 19.

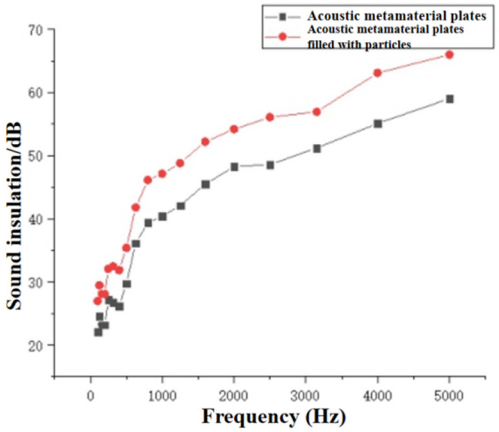


Figure 19. Comparison of the sound insulation of acoustic metamaterials panels before and after filling with particles.

As shown in Figure 19, the acoustic metamaterial panel with particle filling enhances the sound insulation by 4–7 dB across the entire frequency range, significantly improving the overall sound insulation performance. In the frequency range of the ducted fan, the sound insulation of the acoustic metamaterial panel reaches a maximum of 27.2 dB, which increases to 32.5 dB after particle filling, with the overall weighted sound insulation increasing from 37 dB to 42 dB. Additionally, the overall sound absorption performance can be represented by the absorption coefficient curve, as shown in Figure 20. From this figure and the sound insulation curve, it is clear that this solution achieves a comprehensive absorption coefficient of 0.94 for high-frequency noise above 800 Hz, while also effectively absorbing and blocking low-frequency noise.

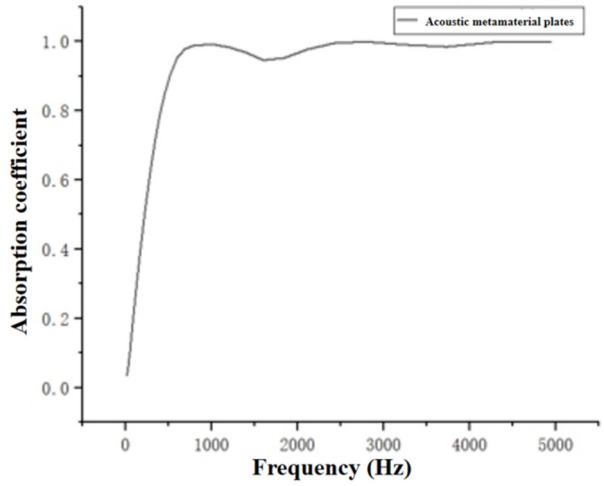


Figure 20. Sound absorption coefficient of acoustic metamaterial panels.

3.3. Simulation Analysis of Rock Wool Sound Absorption and Insulation

The rock wool sound-absorbing and -insulating panel model was imported into COMSOL, and the sound pressure of the noise source based on a tubular belt conveyor was applied to the incident surface. A perfect matching layer was set around the model. The middle layer of the sound-absorbing and -insulating panel was defined as a porous sound-absorbing material and a free mesh was used for discretization. A frequency sweep

from 0 to 5000 Hz with a step size of 100 Hz was conducted. The ratio of incident to reflected sound pressure was calculated to obtain the sound insulation characteristics curve of the rock wool sound-absorbing and -insulating panel. As shown in Figure 21, the rock wool panel exhibits good sound insulation performance below 800 Hz, with a weighted sound insulation level of 30 dB. However, the sound insulation performance at low frequencies is unstable, fluctuating significantly, and unable to maintain a consistently high level.

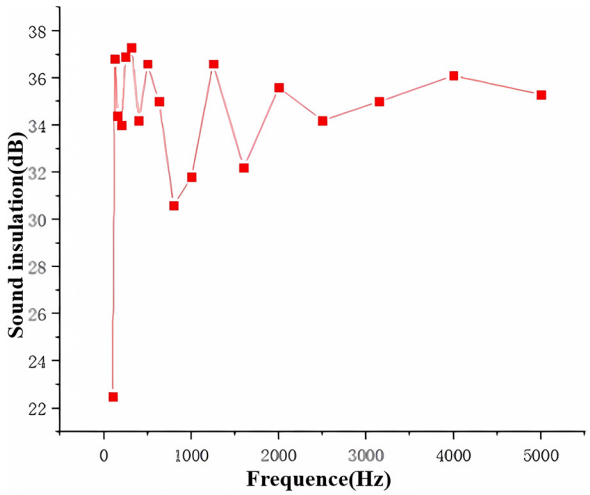


Figure 21. The sound insulation curve of the rock wool sound insulation plate.

The simulation model of the rock wool sound-absorbing and -insulating panel was imported into COMSOL, and the sound pressure of the noise source based on a tubular belt conveyor was applied to the incident surface. A perfect matching layer was set around the panel. The middle layer of the panel was set as a porous sound-absorbing material, and a free mesh was used for discretization while setting the background pressure field. The ratio of incident to reflected sound pressure was calculated to obtain the absorption coefficient curve of the rock wool panel. As shown in Figure 22, the rock wool panel achieves good sound absorption capabilities above 500 Hz, with an absorption coefficient greater than 0.8, indicating its effective sound absorption. However, the panel's ability to absorb low-frequency noise is still limited, making it less effective in solving the full-frequency sound absorption problem.

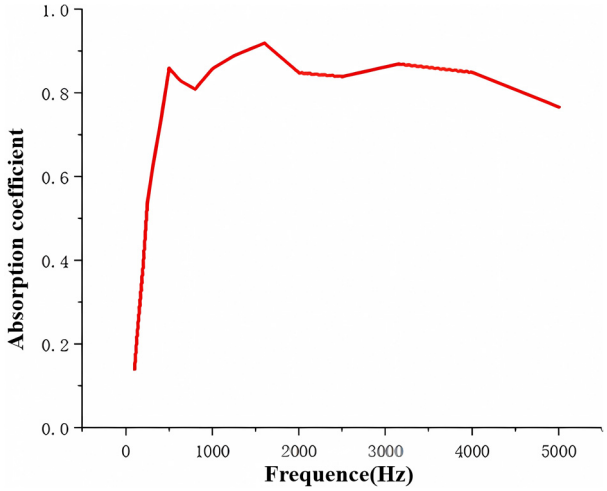


Figure 22. The sound absorption curve of the rock wool sound-absorbing plate.

3.4. Acoustic Testing of Highly Efficient Sound-Absorbing and -Insulating Materials

To validate the accuracy of the simulation data, acoustic tests were conducted on the acoustical superstructure panel, acoustic metamaterial panel, and rock wool sound-absorbing and -insulating panel under the same test conditions. The comparison between simulation and experimental data is shown in Figures 23 and 24.

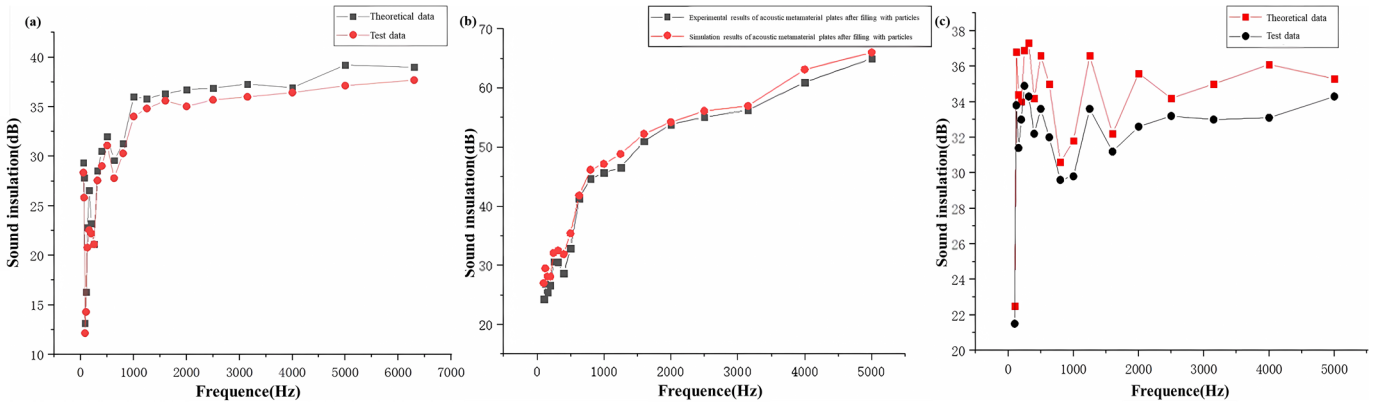


Figure 23. Comparison of sound insulation simulation and test data. (**a**) Acoustic insulation data for the acoustic superstructural panel. (**b**) Sound insulation data for the acoustic metamaterial panel. (**c**) Sound insulation data for the rock wool acoustic insulation panel.

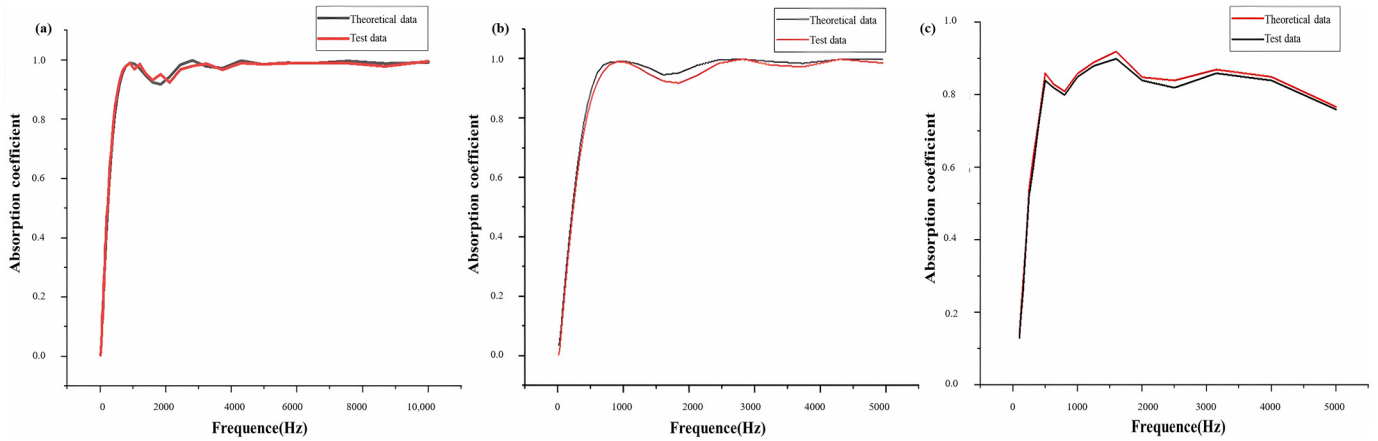


Figure 24. Comparison of sound absorption simulation and test data. (**a**) Acoustic absorption data for the acoustic superstructural panel. (**b**) Acoustic absorption data for the acoustic metamaterial panel. (**c**) Acoustic absorption data for the rock wool acoustic insulation panel.

As shown in Figures 23 and 24, there is some deviation between the experimental and simulated curves for the highly efficient sound-absorbing and -insulating materials. This discrepancy is primarily due to the ideal plane wave conditions set in the finite element simulation, which do not fully match the actual conditions. Additionally, the material parameters used in the simulation are not entirely consistent with the real-world situation. However, the overall trend shows a good alignment between the experimental and simulation curves, confirming the accuracy of the simulation.

At the same time, three kinds of acoustic metamaterial sound insulation were obtained through Figure 23, 36 dB, 42 dB, and 30 dB, showing that the acoustic metamaterials board has the best sound insulation effect. Further, through Figure 24, the acoustic super-structure board and acoustic metamaterials board absorption coefficient at 800 Hz above the high frequency can reach more than 0.9, while the rock wool acoustic panels can only reach

more than 0.8. Through a comprehensive comparison, it can be concluded that the acoustic metamaterials board has the best sound absorption and insulation effect.

3.5. The Acoustic Optimization Design of Highly Efficient Sound-Absorbing Metamaterial Panels

Based on the acoustic simulation designs for the highly efficient sound-absorbing materials, including the superstructure, metamaterial, and rock wool panels, the simulation and experimental results were obtained. The honeycomb-structured acoustic metamaterial exhibited the best sound insulation and absorption performance. Therefore, a simulation was conducted to compare the sound absorption and insulation performance of different panel structures and to identify the optimal structure by comparing the results with the on-site sound insulation measurements.

3.5.1. Impact of Panel Angles on Sound Absorption and Insulation Performance

This section investigates the sound absorption and insulation performance of a honeycomb-structured acoustic metamaterial with different panel angles while keeping the material quantity constant. The metamaterial structure consists of a 1 mm aluminum alloy plate, a 35 mm metamaterial structure, and another 1 mm aluminum alloy plate, giving a total thickness of 37 mm.

Four types of sound-absorbing and -insulating structures were modeled: the length of the flat plate was 3500 mm, and the length of the inclined plate was 693 mm. The angle between the flat plate and the inclined plate was set to 0°, 30°, 60°, and 90°. The inclined plate was oriented toward the side of the tubular belt conveyor. Using the tubular belt conveyor–sound insulation structure analysis method, simulations were conducted for each structure. The sound pressure levels at various monitoring points were calculated using the sound pressure level addition method. The sound pressure level frequency spectrum for each panel angle was plotted and compared with the on-site measurements.

Figure 25 shows the comparison of the sound pressure level frequency spectra for the four inclined panel angle structures. From Figure 25, the sound insulation performance for each structure is summarized in Table 4.

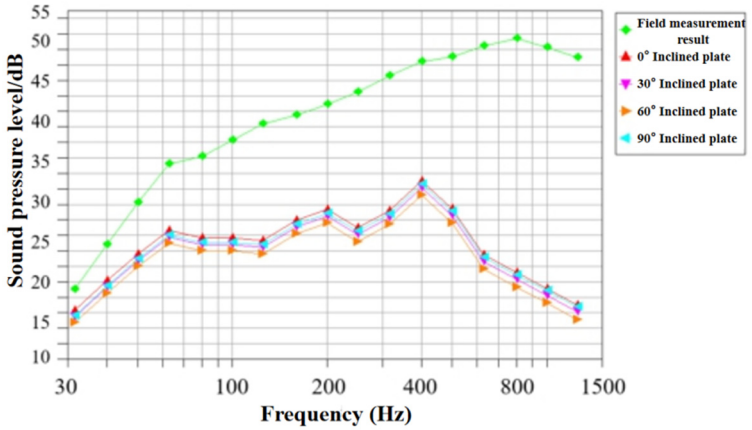


Figure 25. Spectrum diagram of the sound pressure level of sound absorption and insulation structures with different inclined plate angles.

Table 4. Comparison of the sound insulation of acoustic insulation structures with different ramp angles.

Structure	Actual Measurement	0°	30°	60°	90°
Sound pressure level (dB)	58.56	39.09	38.20	37.30	38.62
Sound insulation (dB)	/	19.47	20.36	21.26	19.94

As indicated, the sound pressure level at the monitoring points in residential areas was reduced to below 40 dB under the influence of the honeycomb-structured acoustic metamaterial. The sound insulation performance is highest for the structure with a 60° panel angle, achieving a sound insulation level of approximately 21.26 dB. The 30° structure follows with a sound insulation level of approximately 20.36 dB, and the 90° structure has a sound insulation level of approximately 19.94 dB. The variation in sound insulation performance with different inclined panel angles is relatively small. Therefore, under the condition of using the same material and quantity, the 60° inclined panel angle structure is optimal and was selected for further analysis.

3.5.2. Impact of the Inclined Plate Length on Sound Absorption and Insulation Performance

Based on the previous analysis, the sound absorption and insulation structure with a 60° inclined plate angle was chosen. This section investigates the impact of different material quantities, specifically the inclined plate length, on sound absorption and insulation performance. Three-dimensional models for inclined plates with lengths of 300 mm, 400 mm, 500 mm, 600 mm, 693 mm, 800 mm, and 1000 mm were constructed and simulated. The sound pressure levels at monitoring points for each structure were calculated, and the frequency spectra were plotted for comparison with the on-site measurements.

Figure 26 shows the comparison of the sound pressure level frequency spectra for the seven inclined plate lengths. From Figure 26, the sound insulation performance for each structure is summarized in Table 5.

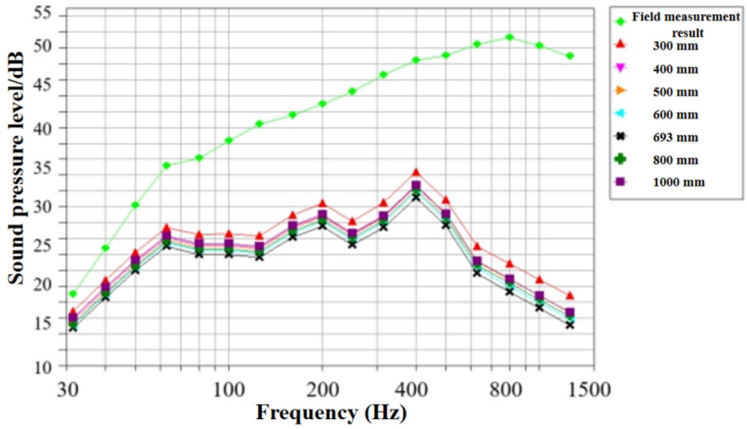


Figure 26. Spectrum diagram of the sound pressure level of absorption and insulation structures with different inclined plate lengths.

Table 5. Comparison of the sound insulation of acoustic insulation structures with different slab lengths.

Structure	Actual Measurement	300 mm	400 mm	500 mm	600 mm	693 mm	800 mm	1000 mm
Sound pressure level (dB)	58.56	40.29	38.66	38.54	37.89	37.30	38.15	38.80
Sound insulation (dB)	/	17.27	19.90	20.02	20.67	21.26	20.41	19.76

The sound pressure levels at monitoring points were reduced to below the emission standard under the influence of the honeycomb-structured acoustic metamaterial. The sound insulation performance was highest for the structure with a 693 mm inclined plate length, achieving a sound insulation level of approximately 21.26 dB. The 600 mm inclined plate structure is followed by a sound insulation level of approximately 20.67 dB. While varying the inclined plate length significantly impacted sound insulation, longer inclined

plates did not necessarily result in better performance. Therefore, the structure with a 693 mm inclined plate length was selected.

Based on the simulation results, considering both the sound insulation effectiveness and material economy, the optimal structure was determined to be the one with a 60° inclined plate angle and a 693 mm inclined plate length.

4. Conclusions

This study conducted simulation research on three types of highly efficient sound-absorbing and -insulating materials—acoustical superstructure panels, acoustic metamaterial panels, and rock wool sound-absorbing and -insulating panels—using COMSOL. Acoustic experiments were then carried out to verify the simulation results. Ultimately, an acoustic optimization design based on honeycomb-structured acoustic metamaterials was proposed as a solution to the noise pollution caused by tubular belt conveyors. At the same time, the study of sound absorption and insulation properties of material panels is of great significance to the economy and society. The main conclusions are as follows:

(1) Through the simulation and test comparison of the three materials, the sound insulation of the acoustic metamaterials board, the acoustic metamaterials board and the rock wool acoustic insulation board are 36 dB, 42 dB and 30 dB, respectively, and the absorption coefficients of the high-frequency 800 Hz and above can reach 0.9, 0.9 and 0.8, respectively, which shows that the acoustic metamaterials board has the best acoustic absorption and sound insulation performance.

(2) The acoustic simulation is validated by acoustic tests to show the feasibility as well as the convenience of acoustic simulation. Through the simulation, many acoustic problems that are difficult to solve by experiments can be solved.

(3) The acoustic metamaterials of the honeycomb structure were simulated and optimized, and the acoustic insulation structure with a ramp angle of 60° and a ramp length of 693 mm was obtained as the optimal structure.

Author Contributions: Conceptualization, X.L., W.X. and Z.C.; Investigation, X.L.; Resources, X.L.; Data curation, H.W.; Writing—review and editing, C.W. All authors have read and agreed to the published version of the manuscript.

Funding: This research received no external funding.

Data Availability Statement: No new data were created or analyzed in this study.

Conflicts of Interest: Authors Xiao Liu and Haopeng Wang were employed by CHN Energy Zhunneng Group Co., Ltd. The remaining authors declare that the research was conducted in the absence of any commercial or financial relationships that could be construed as a potential conflict of interest.

References

1. Ning, X.; Qi, J.; Wu, C.; Wang, W. Reducing noise pollution by planning construction site layout via a multi-objective optimization model. *J. Clean. Prod.* **2019**, *222*, 218–230.
2. Liu, X. Study on Noise Reduction of a Belt Conveyor. *Mech. Manag. Dev.* **2021**, *36*, 325–326.
3. Yi, H. Noise source analysis and noise reduction measures of mining belt conveyor. *Shaanxi Meitan* **2023**, *42*, 91–94.
4. Ji, G.; Huber, J. Recent progress in acoustic metamaterials and active piezoelectric acoustic metamaterial-a review. *Appl. Mater. Today* **2022**, *26*, 101260.
5. Sun, L. Experimental investigation of vibration damper composed of acoustic metamaterials. *Appl. Acoust.* **2017**, *119*, 101–107.
6. Chen, T.; Li, W.; Yu, D. A tunable gradient acoustic metamaterial for acoustic sensing. *Extrem. Mech. Lett.* **2021**, *49*, 101481.
7. Chen, B.; Kong, X.; Chen, C. Study on Sound Insulation Performance of Broadband Membrane-type Acoustic Metamaterials. *Noise Vib. Control* **2024**, *44*, 62–68.
8. Xiang, X.; Lei, Y.; Hu, Z.; Liu, J. Coupling Effect of Local Resonance in Acoustic Metamaterials. *Piezoelectr. Acoustooptics* **2024**, mboxemph46, 586–590.

9. Zhang, Z.; Wang, X.; Liu, Z.Y.; Fan, Q.; Lin, T.R. A study of low frequency sound insulation mechanism of a perforated plate-type acoustic metamaterial. *J. Sound Vib.* **2023**, *558*, 117775.
10. Dogra, S.; Gupta, A. Design, Manufacturing, and Acoustical Analysis of a Helmholtz Resonator-Based Metamaterial Plate. *Acoustics* **2021**, *3*, 630–641. [CrossRef]
11. Jang, J.; Park, C.; Song, K. Lightweight soundproofing membrane acoustic metamaterial for broadband sound insulation. *Mech. Syst. Signal. Pr.* **2022**, *178*, 109270.
12. Iannace, G.; Amadasi, G.; Bevilacqua, A.; Cairoli, M.; Trematerra, A. Resonant Acoustic Metamaterials. *Appl. Sci.* **2024**, *14*, 5080.
13. Xiao, X.; He, Z.C.; Li, E.; Cheng, A.G. Design multi-stopband laminate acoustic metamaterials for structural-acoustic coupled system. *Mech. Syst. Signal Process.* **2019**, *115*, 418–433.
14. Chen, W.; Zhao, X.; Hu, S.; Cao, H.; Lu, L.; Zhou, Z. Simulation of acoustic performance of ceramic foam based on COMSOL. *J. Physics. Conf. Ser.* **2020**, *1650*, 22110.
15. Gong, F.; Li, Q.; Xiao, Z.; Liu, S. Experimental verification of latticed acoustic metamaterials with pentamode to bandgap characteristics. *Eur. Phys. J. B* **2024**, *97*, 192.
16. Zhang, Y.; Wu, C.; Li, N.; Liu, T.; Wang, L.; Huang, Y. Ventilated low-frequency sound absorber based on Helmholtz acoustic metamaterial. *Phys. Lett. A* **2024**, *523*, 129779.
17. Dong, P.; Gong, Q. Simulation analysis of normal incidence acoustic characteristics of sandwich plate based on Comsol. *Ship Sci. Technol.* **2023**, *45*, 56–59.
18. Zhu, X.; Wang, L.; Wang, X.; Jiang, J. Simulation Study of Sound Insulation Performance of the Double-glazed Window. *Noise Vib. Control* **2022**, *42*, 256–262.
19. Wang, J.; Zhou, H. Study on Low Frequency Sound Absorption Mechanism and Regulation Laws of Local Resonant Cavity Coatings. *Noise Vib. Control* **2022**, *42*, 34–39.
20. Lu, Z.; Yu, X.; Lau, S.; Khoo, B.C.; Cui, F. Membrane-type acoustic metamaterial with eccentric masses for broadband sound isolation. *Appl. Acoust.* **2020**, *157*, 107003.
21. Tang, S.; Han, J. Acoustic Propagation Characteristics of Metamaterials with Tubular Structures. *IEEE Access* **2018**, *6*, 72900–72905.
22. Han, J.; Tang, S. Realization of complex curved waveguide based on local resonant 3D metamaterial. *Aip. Adv.* **2018**, *8*, 125327.
23. Liu, H.; Li, L.; Jia, Q.; Jiang, S.; Li, P.; Zhang, X. Radial Seismic Metamaterials Based on Layering Theory: Broadband Shielding of Ultra-Low Frequency Seismic Surface Waves. *Front. Mater.* **2022**, *9*, 908058.

Disclaimer/Publisher's Note: The statements, opinions and data contained in all publications are solely those of the individual author(s) and contributor(s) and not of MDPI and/or the editor(s). MDPI and/or the editor(s) disclaim responsibility for any injury to people or property resulting from any ideas, methods, instructions or products referred to in the content.